

ICP-4D: Bridging Iterative Closest Point and LiDAR Panoptic Segmentation

Gyeongrok Oh¹, Youngdong Jang¹, Jonghyun Choi², Suk-Ju Kang³, Guang Lin⁴, Sangpil Kim^{1,*}

¹Korea University ²Hyundai Motor Company ³Sogang University ⁴Purdue University

Abstract

Dominant paradigms for 4D LiDAR panoptic segmentation are usually required to train deep neural networks with large superimposed point clouds or design dedicated modules for instance association. However, these approaches perform redundant point processing and consequently become computationally expensive, yet still overlook the rich geometric priors inherently provided by raw point clouds. To this end, we introduce ICP-4D, a simple yet effective training-free framework that unifies spatial and temporal reasoning through geometric relations among instance-level point sets. Specifically, we apply the Iterative Closest Point (ICP) algorithm to directly associate temporally consistent instances by aligning the source and target point sets through the estimated transformation. To stabilize association under noisy instance predictions, we introduce a Sinkhorn-based soft matching. This exploits the underlying instance distribution to obtain accurate point-wise correspondences, resulting in robust geometric alignment. Furthermore, our carefully designed pipeline, which considers three instance types—static, dynamic, and missing—offers computational efficiency and occlusion-aware matching. Our extensive experiments across both SemanticKITTI and panoptic nuScenes demonstrate that our method consistently outperforms state-of-the-art approaches, even without additional training or extra point cloud inputs.

1. Introduction

Autonomous driving systems heavily depend on precise perception of dynamic 3D environments with geometrically accurate measurements captured by LiDAR sensors. In particular, LiDAR segmentation plays a crucial role in enabling comprehensive point-wise understanding. In 3D environments, LiDAR panoptic segmentation [19, 32] originates from semantic and instance segmentation, which jointly identify class categories and instance IDs. Along with the recent significant advances in frame-wise perception, 4D LiDAR panoptic segmentation [2] has emerged to capture temporal

relationships in a holistic manner. In this context, ensuring temporal continuity is a principal purpose in 4D LiDAR panoptic segmentation, even under instance motions.

With its potential benefits, as shown in Figure 1, the mainstream of prior works can be categorized into three discrete paradigms: 1) IoU-based association, 2) Query-propagated association, and 3) Detect & Track association. One solution [2, 16, 20, 54, 63], superimposing point clouds, is widely adopted for establishing 4D spatio-temporal volume. It enables consistent instance tracking over time by measuring the overlapped regions (see Figure 1(a)). However, despite its simplicity, stacking point clouds (i.e., increasing the number of points per batch) leads to a quadratic growth in computational overhead, which is an inherent challenge in point cloud processing [22, 28, 50, 51].

An alternative direction [1, 29, 30] seeks to mitigate this issue by treating each scan independently, as illustrated in Figure 1(b) and 1(c). They are primarily derived from the two major paradigms of multi-object tracking, tracking-by-detection [7, 36, 49, 58] and query propagation [31, 55, 59], to assign consistent IDs for instances. Both approaches differ substantially in training strategies, yet commonly suffer from error accumulation [41, 59] and reliance on costly and dataset-dependent training. Consequently, we argue that this suboptimal design fails to fully exploit the strong perception capability of 3D panoptic networks, which naturally raises the following question: *Can instance association be achieved efficiently using only a 3D panoptic network?*

To answer this, we propose Iterative Closest Point (ICP)-based strategy for reliable instance matching, even without any training process. ICP is widely used for point cloud registration [11, 46, 57], but its applicability beyond that has been largely underexplored. Here, we first integrate ICP into the 4D LiDAR panoptic segmentation framework. This allows explicit mapping through estimated transformation between instance segment pairs in successive scans. While this mapping works well with complete segment pairs, noisy predictions hinder finding corresponding points via nearest-neighbor approach, as it ignores the global instance structure. To handle this, we propose *Sinkhorn-based soft matching* that strengthens the robustness against outliers

*Corresponding author.

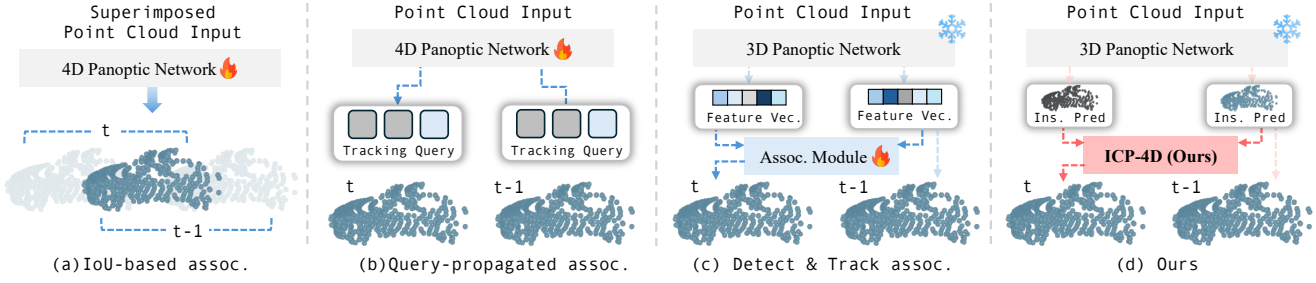


Figure 1. Comparison of 4D LiDAR panoptic segmentation methods: (a) IoU-based, (b) Query-propagated, (c) Detect & Track, and (d) ICP-4D. Instead of relying on training with large-scale point clouds, ours achieves reliable association in a fully training-free manner. 🔥 indicates methods that *require training* and ❄️ denotes *frozen network*.

with instance-aware correspondences. Specifically, we represent each instance’s point set as a probability distribution. Then, the correspondence problem is cast as a Sinkhorn Optimal Transport (OT) problem [12], which computes an entropy-regularized transport plan between the two distributions. This plan identifies point pairs that minimize the transportation cost, thereby establishing soft correspondences.

ICP demonstrates competitive performance in instance association. However, its iterative mechanism and the physical limitations of LiDAR sensors introduce remaining challenges, a marginal increase in runtime and vulnerability to occlusion. Given these limitations, we classify instances into three categories: static, dynamic, and missing. For associating static instances, we employ its point set statistics (i.e., mean and covariance) considering the rigid property. This significantly reduces the number of matching candidates and preserves computational efficiency. Moreover, to compensate for occluded instances, we present a memory bank to store prediction results within a short temporal window.

To wrap it up, we named our overall pipeline as ICP-4D and demonstrate its effectiveness through extensive experiments on the SemanticKITTI [4] and nuScenes [13] benchmarks. Note that ICP-4D achieves superior performance over existing state-of-the-art methods and ranks 1st on the SemanticKITTI test leaderboard, even under the minimal setting of a single scan and without any additional training.

The contributions of this work are summarized as follows:

- We introduce ICP-4D that is a novel training-free 4D LiDAR panoptic segmentation pipeline, flexibly integrated with a wide range of 3D panoptic segmentation networks.
- We propose a Sinkhorn-based soft matching strategy to enhance the robustness of point correspondences, and we delicately design instance state-conditioned solutions to effectively mitigate time complexity and occlusion.
- Extensive experiments in challenging environments clearly demonstrate the superiority of ICP-4D, supported by in-depth analysis.

2. Related Work

2.1. LiDAR Panoptic Segmentation

LiDAR panoptic segmentation simultaneously handles two different basis tasks, semantic and instance segmentation. In early, proposal-based methods [27, 34, 52] filter the background points with Mask R-CNN [14]’s semantic head, then group the *thing* points into instances. In contrast, proposal-free methods [15, 25, 37, 62] independently predict semantic prediction and class-agnostic instance segments via end-to-end training manners. 4D LiDAR panoptic segmentation extends these frameworks to sequential scans, requiring instance IDs to remain consistent over time.

In terms of association strategy, predominant works [2, 16, 20, 54, 60, 63] aggregate consecutive point clouds (e.g., 2-4 scans) and group instances in overlapping regions to ensure temporal continuity. Alternatively, CA-Net [29] associates instances via feature-wise similarity, followed by the outputs of 3D panoptic network. Mask4D [30] preserves identity consistency across scans by iteratively updating the track queries in an end-to-end manner. Despite these attempts, we observe significant issues regarding the computational cost and limited adaptability (see Sec. 1). Instead, we propose ICP-4D that is a flexible, efficient, and well-balanced instance association through direct geometric registration.

2.2. Multi-Object Tracking (MOT)

MOT is an indispensable task for autonomous driving systems, enabling the tracking of all detected objects across scans. Tracking-by-detection (TBD) paradigm [7, 36, 49, 58] has become the *de facto* standard due to its simplicity and the rapid progress of detectors. Here, the motion model (e.g., Kalman Filter [18]) plays a key role by estimating future object states to maintain tracking continuity. The emergence of DETR [64] has recently drawn increasing attention to the end-to-end paradigm [31, 55, 59], which performs detection and tracking in parallel using query-based tracking. These paradigms are not confined to 2D images but are increasingly embraced in 3D autonomous driving scenarios [35, 48, 56, 61] as well. However, despite sharing objectives with MOT, 4D LiDAR panoptic segmentation dif-

fers fundamentally, as it requires holistic point-level scene understanding instead of bounding boxes. Although ICP-4D follows the TBD paradigm, it operates directly on point-level panoptic outputs, enabling instance association grounded in the geometric structure of the underlying point clouds.

2.3. Iterative Closest Point (ICP)

ICP [6] is one of the most well-established and widely adopted algorithm for point-set registration [9, 24, 39]. Over the years, many variants of the vanilla ICP have been proposed to address its limitations, and have been widely adopted in both traditional engineering [8, 38, 40, 53] and deep learning-based applications [11, 46, 57]. Nowadays, ICP-Flow [26] proposes a compelling scene flow prediction framework that inspired this work. They only consider point-wise motion estimation between two temporally adjacent scans by leveraging well-separated instance clusters. In this paper, we introduce ICP into the context of the 4D LiDAR panoptic segmentation, ensuring the temporal continuity of instances across the entire scans. Remarkably, our Sinkhorn-based soft matching enables instance-centric association, even when predictions are noisy, imprecise, or fragmented.

3. Method

ICP-4D primarily focuses on ensuring temporal continuity of the instances in an unsupervised manner. To handle this, we adopt Iterative Closest Point (ICP) [6] to associate instances through their geometric consistency over time. In this section, we first provide the introductory ICP (Sec. 3.1), then go over the technical details of our methods (Sec. 3.2).

3.1. Preliminary

Iterative Closest Point (ICP). Conventionally, for point cloud registration, ICP estimates the optimal transformation by iteratively minimizing the difference between source and target point sets. Given two point sets $\mathcal{P}_{src} \in \mathbb{R}^{n \times 3}$ and $\mathcal{P}_{dst} \in \mathbb{R}^{m \times 3}$, it starts with the initial guess of rigid transformation $(\mathbf{R}^{(0)}, \mathbf{t}^{(0)})$, where the rotation $\mathbf{R} \in \text{SO}(3)$ and translation $\mathbf{t} \in \mathbb{R}^3$, which satisfies the following formula:

$$\mathcal{P}_{dst} \approx \mathbf{R}\mathcal{P}_{src} + \mathbf{t}. \quad (1)$$

Here, in order to compute the alignment error, pairwise correspondences are established using a nearest-neighbor search algorithm (e.g., KD-tree [5]). Classical ICP adopts l_2 distance as the error metric between the matched point pairs. Ultimately, the optimal rigid transformation is obtained by iteratively solving a series of least-squares problems as:

$$\arg \min_{\mathbf{R}, \mathbf{t}} \|\mathbf{R}\mathcal{P}_{src} + \mathbf{t} - \mathcal{P}_{dst}\|^2, \quad (2)$$

to update the rotation \mathbf{R} and translation \mathbf{t} until convergence. With this theoretical background, we investigate how ICP contributes to consistent instance ID assignment across frames while enhancing robustness against outliers.

3.2. ICP-4D

Our proposed ICP-4D is developed on top of a pre-trained 3D LiDAR panoptic segmentation model [15, 54], which is specialized in frame-wise perception. Through this model, we obtain the per-point instance and semantic prediction $(\mathcal{I}_i, \mathcal{S}_i)$ for a given point cloud with N points, where $\mathcal{S}_i \in \{1, \dots, C\}$, $\mathcal{I}_i \in \mathbb{N}_0$, and C is the number of classes. Prior to the association stage, we construct a set of matching candidates between t and $t - 1$ times by pairing source and destination instances as follows:

$$\mathcal{G}_{src} \times \mathcal{G}_{dst} = \{(a_i, b_j) \mid a_i \in \mathcal{G}_{src}, b_j \in \mathcal{G}_{dst}\}, \quad (3)$$

where \mathcal{G}_{src} and \mathcal{G}_{dst} are respectively denoted as the sets of unique instance IDs in the source and destination. Then, we derive the filtered set $\mathcal{M} = \mathcal{G}'_{src} \times \mathcal{G}'_{dst}$ by keeping only the pairs in $\mathcal{G}_{src} \times \mathcal{G}_{dst}$ that share the same semantic class. In this study, we categorize instances into dynamic, static, and missing types to facilitate effective instance association across frames.

3.2.1. Static Instance

Under the assumption that both the center and the shape of a non-moving rigid object remain invariant, we filter static instances based on their centers and further refine them using covariance cues to improve selection fidelity. Given the matching candidates \mathcal{M} , we first represent each instance by the set of 3D points belonging to it. For all instances in \mathcal{G}'_{src} and \mathcal{G}'_{dst} , we denote their corresponding point sets as $P(\mathcal{G}'_{src})$ and $P(\mathcal{G}'_{dst})$, respectively. Then, we compute the center of each point set:

$$\mu_s = \frac{1}{|P(\mathcal{G}'_{src})|} \sum_{u \in P(\mathcal{G}'_{src})} u, \quad \mu_d = \frac{1}{|P(\mathcal{G}'_{dst})|} \sum_{v \in P(\mathcal{G}'_{dst})} v, \quad (4)$$

where $u, v \in \mathbb{R}^3$ and indicate the world coordinates of points. We keep only the pairs satisfying $\|\mu_d - \mu_s\|_2 < \tau_{center}$, where τ_{center} is the distance threshold for identifying non-moving objects based on center consistency. Although this naive approach performs well under ideal conditions, it suffers when applied to noisy predicted point sets, resulting in unsuitable pair associations. Thus, we introduce an additional covariance-based constraint that measures the similarity of the spatial spread and geometric structure of the instance point sets. Specifically, the covariance of each point set is computed as follows:

$$\sigma_s = \text{Cov}(P(\mathcal{G}'_{src})), \quad \sigma_d = \text{Cov}(P(\mathcal{G}'_{dst})). \quad (5)$$

To assess shape consistency, we measure the similarity between the two covariance matrices and use the predefined threshold τ_{cov} to control the discrepancy between source and destination point set:

$$\frac{\|\sigma_d - \sigma_s\|_F}{\text{tr}(\sigma_d) + \text{tr}(\sigma_s)} < \tau_{cov}, \quad (6)$$

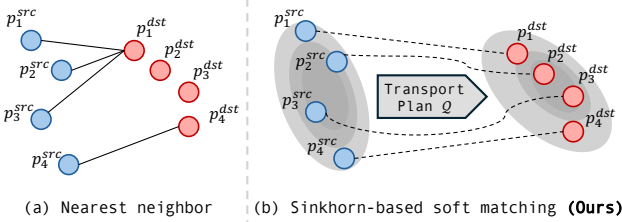


Figure 2. **Illustration of Sinkhorn-based soft matching.** (a) Nearest neighbor-based matching aligns each source point with its closest counterpart, focusing only on local point proximity. (b) In contrast, correspondences are computed by transport plan \mathcal{Q} , enabling instance-aware matching that respects the global geometry of each instance point set.

where $\text{tr}(\cdot)$ and $\|\cdot\|_F$ denote the matrix trace and the Frobenius norm. Then, based on the obtained similarity scores, we choose the highest score for each source instance to find the best-matching pairs while avoiding duplicate associations.

3.2.2. Dynamic Instance

After filtering static instances, the remaining candidates $\mathcal{G}_{\text{src}}''$ and $\mathcal{G}_{\text{dst}}''$ are fed into the ICP loop that is the core mechanism of our framework that enables instance association without any supervised training. In the vanilla ICP loop, the first step is finding point pairs to compute the distance by utilizing the nearest-neighbor algorithm [5]. While ICP has a powerful ability of registering point cloud sets, determining the corresponding points under noisy instance predictions potentially causing erroneous matches. Therefore, we propose a *Sinkhorn-based soft matching* scheme that facilitates stable correspondence estimation within the ICP framework.

Sinkhorn-based Soft Matching. Sinkhorn-based soft matching starts from regarding the point cloud as a probability distribution rather than discrete set of individual points. Given two point sets $P(\mathcal{G}_{\text{src}}'') = \{u_i\}_0^{I-1}$ and $P(\mathcal{G}_{\text{dst}}'') = \{v_j\}_0^{J-1}$, where I and J denote the number of points in each segment, we formulate correspondence estimation as an Optimal Transport (OT) problem [12]. Specifically, we seek a transport plan \mathcal{Q} that minimizes the cost of transforming one distribution into the other as follows:

$$\text{OT}(P(\mathcal{G}_{\text{src}}''), P(\mathcal{G}_{\text{dst}}'')) := \min_{\mathcal{Q}} \langle \mathcal{Z}, \mathcal{Q} \rangle_F - \epsilon H(\mathcal{Q}), \quad (7)$$

where $\langle \cdot \rangle_F$ denotes Frobenius dot-product. Here, cost matrix \mathcal{Z} represents the pairwise transport cost, defined as $\mathcal{Z}_{ij} = \|u_i - v_j\|_2^2$. The entropy H and ϵ control the smoothness of the transport plan as a regularization term. Then, we utilize the Sinkhorn-Knopp algorithm [42] that provides an efficient solution to the entropy-regularized optimal transport problem by iteratively rescaling the rows and columns of the transport plan \mathcal{Q} until the marginal constraints are satisfied. Afterwards, we derive the final correspondences from the source to the destination point by taking the argmax

operation over each row of \mathcal{Q} . That is, we approximate point-to-point correspondences by selecting the highest transport probability from the minimized transport plan. As a result, this strategy is based on considering the instance instead of local points (see Figure 2), thereby alleviating the vulnerability to outliers and incorrect predictions.

Returning to the ICP procedure, we follow the standard process, initializing transformations with a histogram-based method [26] to reduce sensitivity to initial estimates and subsequently running iterative refinement to get the final rigid transformation. After obtaining the transformation, we determine whether two instances correspond by evaluating the IoU between their transformed point sets. Specifically, points with errors smaller than the predefined threshold τ_{dist} are treated as inliers. Then, in order to filter valid matching candidates, we evaluate alignment accuracy between source and destination instances by IoU scores as follows:

$$\mathcal{M}^{\text{dyn}} = \begin{cases} \text{matched, if } \langle \mathcal{F}(P(\mathcal{G}_{\text{src}}'')), P(\mathcal{G}_{\text{dst}}'') \rangle \geq \tau_{\text{iou}}, \\ \text{rejected, otherwise,} \end{cases} \quad (8)$$

where $\langle \cdot \rangle$ denotes the IoU calculation, and \mathcal{F} applies the estimated transformation obtained by ICP.

Option: Bijective assignment. A naive approach is to pair each source instance with its most similar target instance; however, it fails to enforce one-to-one correspondence. Thus, we derive a transformation-aware matching cost that integrates the ICP results—rotation \mathbf{R} , translation \mathbf{t} , and the IoU score s_{iou} . Formally, the matching cost \mathcal{C} of dynamic matching pairs $(i, j) \in \mathcal{M}^{\text{dyn}}$ is defined as:

$$\begin{aligned} \mathcal{C}_{ij} &= \gamma_t c_{ij}^{(t)} + \gamma_r c_{ij}^{(r)} + \gamma_s c_{ij}^{(s)}, \\ c_{ij}^{(t)} &= \|\mathbf{t}_{ij}\|_2, \quad c_{ij}^{(r)} = \|\theta_{ij}\|_2, \quad c_{ij}^{(s)} = \|1 - s_{\text{iou}}\|_2, \end{aligned} \quad (9)$$

where θ denotes the axis-angle rotation vector obtained from \mathbf{R} . We normalize each cost term to comparable scales before weighting so that γ_t , γ_r , and γ_s control their relative contributions. By minimizing \mathcal{C} with the Hungarian algorithm [21], we obtain a bijective assignment that considers the geometric alignment.

3.2.3. Missing Instance

Occlusions stemming from the inherent limitations of LiDAR sensor often break temporal continuity beyond two consecutive scans. To mitigate this, we introduce a memory bank \mathcal{B} that caches the world coordinates, semantic labels, and instance IDs of unmatched objects. Owing to bounded memory capacity, \mathcal{B} keeps only entries observed within a short window of the previous w_{mem} scans. If \mathcal{B} is nonempty, we retrieve previously stored instance information and associate using the dynamic instance matching process.

Table 1. **Quantitative results on SemanticKITTI benchmark [4].** We highlight the best scores in **bold** and the underline indicates the second-best scores. Note that * represents that the results are obtained from our implementation following the official training setup.

Method	# Scan	Assoc. Training	Validation set					Test set				
			LSTQ	S_{assoc}	S_{cls}	IoU^{St}	IoU^{Th}	LSTQ	S_{assoc}	S_{cls}	IoU^{St}	IoU^{Th}
(a) IoU-based Association												
4D-PLS [2]	4	\times	62.7	65.1	60.5	65.4	61.3	56.9	56.4	57.4	66.9	51.6
4D-STOP [20]	4	\times	67.0	74.4	60.3	65.3	60.9	63.9	69.5	58.8	67.7	53.8
Eq-4D-STOP [63]	4	\times	70.1	<u>77.6</u>	63.4	66.4	67.1	67.0	72.0	62.4	69.1	60.9
Mask4Former [54]	2	\times	70.5	74.3	66.9	67.1	66.6	<u>68.4</u>	67.3	69.6	72.7	65.3
(b) Query-propagated Association												
Mask4D [30]	1	\checkmark	<u>71.4</u>	75.4	67.5	65.8	69.9	64.3	66.4	62.2	69.9	52.2
(c) Detect & Track Association												
KPConv [43]+PP [23]+MOT [47]	1	\checkmark	46.3	37.6	57.0	64.2	54.1	38.0	25.9	55.9	66.9	47.7
KPConv+PP+SFP [33]	1	\checkmark	46.0	37.1	57.0	64.2	54.1	38.5	26.6	55.9	66.9	47.7
DS-Net [15]	1	-	-	-	63.5	64.6	62.0	-	-	60.6	66.9	52.0
+ CA-Net [29]	1	\checkmark	67.4	71.6	63.5	64.6	62.0	62.1	63.7	60.6	66.9	52.0
+ ICP-4D (Ours)	1	\times	68.5 <small>(+1.1)</small>	74.0 <small>(+2.4)</small>	63.5	64.6	62.0	62.9 <small>(+0.8)</small>	65.3 <small>(+1.6)</small>	60.6	66.9	52.0
Mask4Former*	1	-	-	-	67.5	65.2	70.6	-	-	70.5	72.7	67.4
+ CA-Net*	1	\checkmark	70.4	73.4	67.5	65.2	70.6	66.5	62.8	70.5	72.7	67.4
+ ICP-4D (Ours)	1	\times	72.7 <small>(+2.3)</small>	78.3 <small>(+4.9)</small>	67.5	65.2	70.6	70.3 <small>(+3.8)</small>	<u>70.0</u> <small>(+7.2)</small>	70.5	72.7	67.4

Table 2. **Quantitative results on panoptic nuScenes [13].**

Method	# Scan	LSTQ	S_{assoc}	S_{cls}	IoU^{St}	IoU^{Th}
(a) IoU-based Association						
4D-Stop [20]	4	60.5	62.5	58.6	74.4	54.9
Eq-4D-Stop [63]	4	67.3	73.7	61.5	76.4	58.7
Mask4Former* [54]	2	<u>67.6</u>	63.0	72.5	76.6	66.3
(b) Query-propagated Association						
Mask4D* [30]	1	58.5	54.1	63.1	75.5	55.7
(c) Detect & Track Association						
Mask4Former*	1	-	-	71.0	76.0	65.9
+ CA-Net [29]*	1	63.4	56.6	71.0	76.0	65.9
+ ICP-4D (Ours)	1	67.9	<u>65.0</u>	71.0	76.0	65.9

4. Experiments

4.1. Experiment Setup

Datasets. We choose two representative benchmarks. SemanticKITTI [4] captures point clouds using a 64-beam LiDAR at 10 Hz and provides point-wise annotations for 19 semantic classes (8 Things / 11 Stuff). In contrast, panoptic nuScenes [13] uses a 32-beam LiDAR operating at 2 Hz and offers point-wise annotations for 16 semantic classes (10 Things / 6 Stuff). This contrast serves as a valuable testbed for assessing generalization across dense (SemanticKITTI) and sparse (nuScenes) LiDAR settings.

Evaluation Metrics. To evaluate both tracking and segmentation quality, we adopt the widely used LSTQ metric [2], defined as $LSTQ = \sqrt{S_{cls} \times S_{assoc}}$. Here, S_{cls} measures how accurately semantic labels are assigned and S_{assoc} evaluates how consistently instance identities are maintained throughout the sequence, independently of semantic accu-

racy. However, S_{assoc} is computed only from true positive associations weighted by IoU scores. Thus, when prediction masks are stable and yield high IoU scores, ID switch causes a sharper drop in this score. Consequently, while ICP-4D primarily influences S_{assoc} , the LSTQ must be taken into account as a meaningful indicator of temporal consistency.

Implementation Details. Our proposed ICP-4D can be incorporated into any 3D LiDAR panoptic segmentation network. For fair comparison, we basically follow two baseline’s configuration, DS-Net [15] and Mask4Former [54]. Since Mask4Former is originally developed for 4D panoptic segmentation, we train it using the official settings with the input modified to a single scan instead of multiple sweeps. For instance association, thresholds for filtering instance pairs are set to $\tau_{center} = \tau_{cov} = \tau_{dist} = 0.1$ and $\tau_{iou} = 0.2$. Additionally, the short window w_{mem} is set to 3 for missing instances, the regularization parameter for optimal transport is set to $\epsilon = 0.2$, and the number of ICP iterations is fixed to 30. All experiments are conducted on a single RTX A6000.

4.2. Quantitative Analysis

4.2.1. 4D LiDAR Panoptic Segmentation Results

SemanticKITTI. Table 1 reports the experimental results on SemanticKITTI validation and hidden test set. Here, we clearly observe two insights. First, ICP-4D achieves the highest LSTQ score across all data split regardless of the number of input scans. Specifically, while (a) IoU-based association approaches rely on 2-4 more input point clouds, our ICP-4D achieves superior performance using only a single scan, showing improvements of up to 13.2 percent points in S_{assoc} and 10.0 percent points in LSTQ. Furthermore,

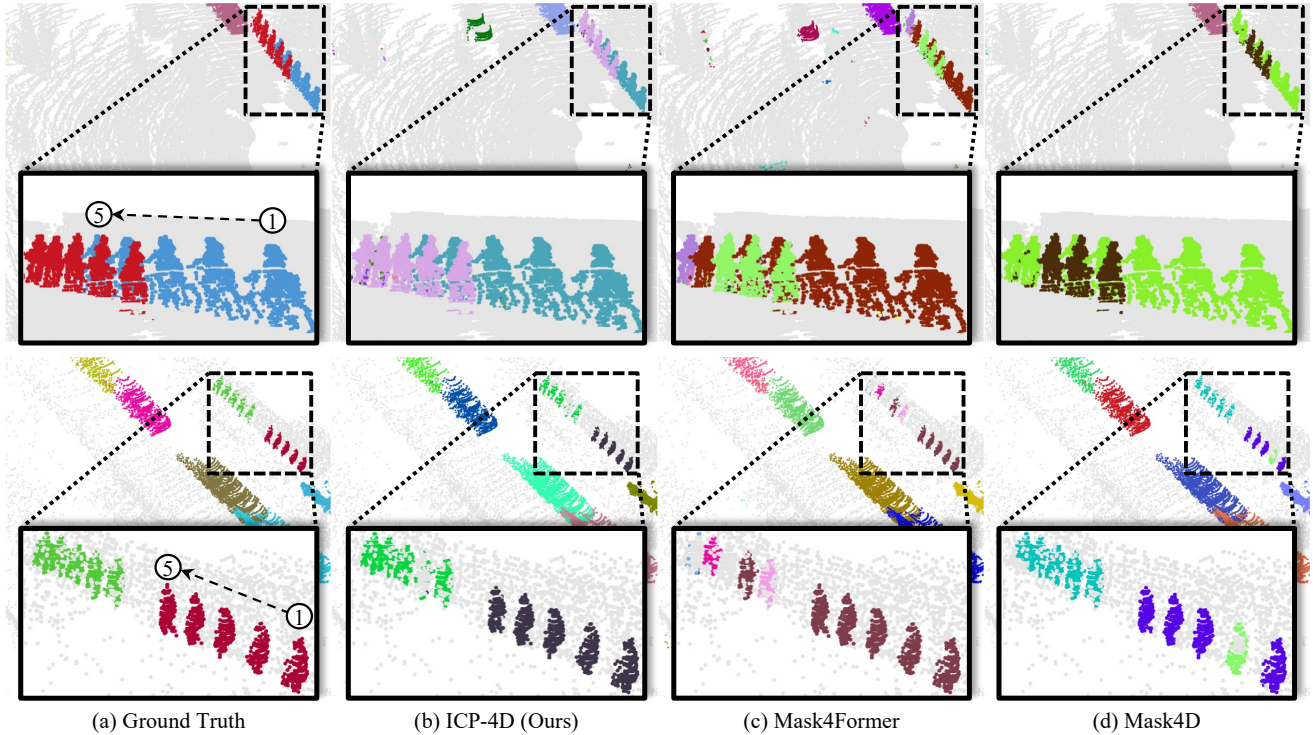


Figure 3. **Qualitative comparison on SemanticKITTI validation set.** We visualize the association results over five consecutive scans for both the baselines and our ICP-4D. Different colors represent different instances. The dotted boxes zoom in for clear comparison. For clarity, we use circled numbers (1–5) to represent the frame indices.

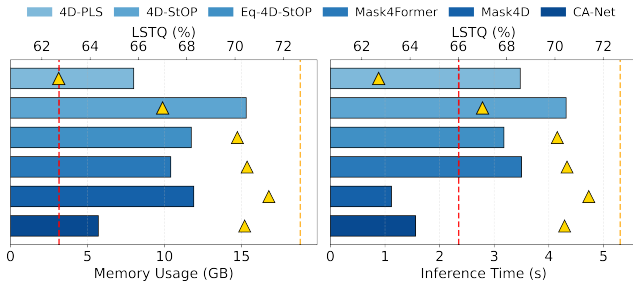


Figure 4. **Comparison of computational efficiency.** We illustrate the efficiency trade-offs between memory usage (left) & runtime (right) and performance across different methods. Yellow triangles show LSTQ scores for each model. Red dashed line denotes our memory & runtime, and yellow dashed line marks our LSTQ score.

by comparing with the learning-based approaches (b) and (c), another noticeable aspect is that ICP-4D consistently outperforms recent state-of-the-art methods on both the validation and test sets, whereas Mask4D and CA-Net drop in performance on the test set. This highlights the robustness of our direct geometric registration with raw point clouds, rather than relying on training-dependent feature association.

nuScenes. Table 2 shows the 4D panoptic results on panoptic nuScenes dataset. Consistent with the observations on the

SemanticKITTI dataset, ICP-4D delivers notably stronger instance association performance, outperforming existing methods in terms of LSTQ. It is important to note that baselines generally suffer when the LiDAR scans are captured with a long interval. In such scenarios, multi-scan aggregation benefits from denser temporal support and thus exhibit strong performance. For example, EQ-4D-StOP with 4 aggregated scans surpasses Mask4Former with 2 scans by a substantial margin in the association metric. Nevertheless, our ICP-4D demonstrates that even without accessing multiple scans, a single-scan input is sufficient to achieve competitive performance. This result implies that ICP-4D remains highly effective even under sparse LiDAR configurations.

4.2.2. Comparison of Efficiency

Next, we examine computational efficiency in terms of memory usage and runtime. For each method, we report the peak GPU memory consumption and the average runtime measured over the entire validation set. Figure 4 illustrates the results, supporting that ICP-4D offers a most well-balanced trade-off between performance and computational overhead. First, when compared with the IoU-based association approaches, we observe that ICP-4D requires 60.7%–79.4% less memory and achieves a 26.1%–45.6% runtime efficiency improvement, all while delivering superior LSTQ perfor-

Table 3. **Ablation on module design.**

Exp. #	Method			Metric	
	Hist. Init.	Sink. Soft Matching	Memory Bank	LSTQ	S_{assoc}
1	-	-	-	70.1	73.4
2	✓	-	-	71.3	75.4
3	-	✓	-	71.4	75.6
4	✓	✓	-	72.0	76.8
5	✓	✓	✓	72.7 (±2.6)	78.3 (±4.9)

Table 4. **Ablation study on different types of instances.**

Instance Type			Metric		
Static	Dynamic	Missing	LSTQ	S_{assoc}	Inf. time (s)
✓	-	-	35.4	18.5	1.06
-	✓	-	71.8	76.7	3.98
✓	✓	-	72.0	76.8	2.06 (−48.2%)
✓	✓	✓	72.7	78.3	2.35 (−41.0%)

mance. While Mask4D exhibits high efficiency in runtime, it inevitably incurs substantial memory overhead due to its transformer-based architecture design. Lastly, CA-Net is computationally efficient; however, it fails to obtain reliable association performance. This gap is already observable on the validation set and becomes even more pronounced on the hidden test set, as highlighted in blue in Table 1.

4.3. Qualitative Analysis

In this section, we deeply analyze the effectiveness of ICP-4D qualitatively by presenting the visualization results in Figure 3. In the first row, there are two bicyclists riding in a line. Both ground truth and our ICP-4D consistently distinguish the two bicyclists across time. However, Mask4Former struggles to preserve identity consistency when objects are spatially adjacent or overlapping due to its IoU-based association. Furthermore, Mask4D employs learnable tracking queries for association, which can lead to confused tracking queries when objects share similar visual or spatial features. Then, in the second row, we emphasize the effectiveness of our memory bank in handling missing instances. Even when the 3D panoptic model fails to detect the person colored in green at the second time step, the memory bank successfully retrieves the missing instance and preserves its identity across scans. In contrast, Mask4Former experiences ID switching when it fails to detect instance due to the absence of the overlapped region. Consequently, these observations underscore the importance of explicit geometric matching in our approach and a well-structured association pipeline.

4.4. Ablation Study

Module Design. Table 3 shows the effects of our proposed methods. Exp. #1 directly applies the vanilla Iterative Closest Point (ICP) for associating instances, serving as a baseline to examine the feasibility of ICP in an unsupervised manner. Despite its strong matching capability, ICP is highly sensitive to the quality of initial alignment. In Exp. #2, we

Table 5. **Ablation on matching strategy.**

Method	LSTQ	S_{assoc}	S_{cls}
Hungarian Matching	72.3	77.6	67.5
Greedy Matching	72.7	78.3	67.5

Table 6. **Ablation on DBSCAN instance refinement.**

Method	LSTQ	S_{assoc}	S_{cls}	Inf. Time (s)
w/o DBSCAN [10]	71.8	75.8	67.5	0.84
w/ DBSCAN	72.7	78.3	67.5	2.35

observe a little performance gain when applying histogram-based initialization proposed by [26], which stabilizes the initial alignment. Notably, our Sinkhorn-based soft matching brings further improvements without the influence of initial pose (see Exp. #3). The key takeaway is that instance-aware correspondence to alleviate the instability of local point matching is highly beneficial for obtaining reliable matching points between noisy instance segments, and as a result helps to estimate an accurate transformation. Exp. #4 demonstrates that coupling these components yields a complementary effect, leading to more robust instance association and improved overall performance. Lastly, Exp. #5 demonstrates the effectiveness of incorporating a memory bank for handling occluded and missing instances, resulting in superior performance.

Effect of Different Types of Instances. To validate our carefully designed pipeline with respect to different instance types, Table 4 presents the association results and average inference time per a single scan. First, we employ the association strategy designed for static instances (Sec. 3.2.1) to matching candidates over all detected objects. Despite requiring minimal computation, only a small subset of instances remain consistently tracked, 18.5 percent points indicating that static cues alone are insufficient for reliable association. In contrast, relying solely on dynamic instance association (Sec. 3.2.2) achieves high performance, but is computationally expensive. Thus, combining these strategies reduces the runtime by 48.2% while simultaneously improving performance, as it significantly narrows the matching candidates for dynamic instance association. Consequently, our full ICP-4D enhances the tracking continuity without sacrificing computational efficiency.

Analysis of Matching Strategy. In Table 5, we compare the performance of ICP-4D with one-to-one or greedy matching. The evaluation is done using SemanticKITTI validation set and set all $\gamma_{\{t,r,s\}} = 1$ for the Hungarian matching. We observe that greedy matching surpasses the bijective matching by a small margin in S_{assoc} . We interpret this gap as being caused by segmentation noise, where a single object is often predicted as multiple disjoint segments. In such case, the greedy strategy adapts to this variability, resulting in more

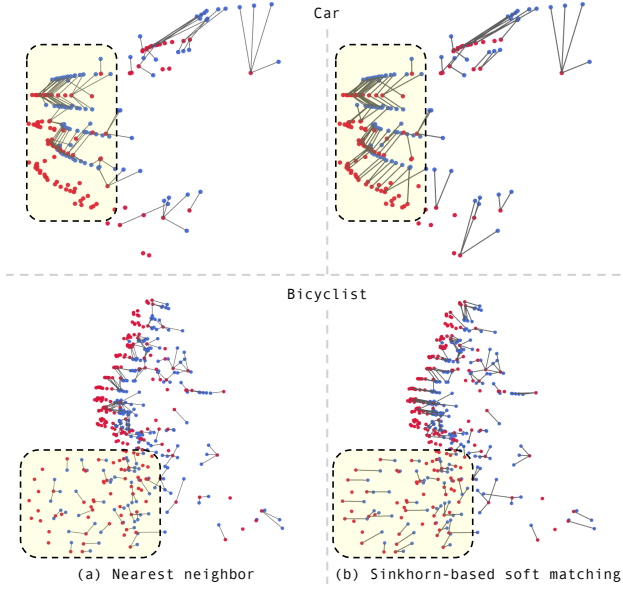


Figure 5. **Point-wise correspondence visualization.** Visualization of point-wise correspondences is provided to illustrate the effect of the Sinkhorn-based soft matching. • and ● represent the target and source points, respectively.

robust temporal consistency. However, as segmentation quality improves, bijective matching becomes advantageous for maintaining unique and consistent identities.

Analysis of DBSCAN Instance Refinement. In this specific experiment of integrating ICP-4D with Mask4Former, we apply DBSCAN clustering [10] as done in the original Mask4Former setting. Table 6 summarizes the results, where we derive two major insights. First, ICP-4D consistently surpasses existing state-of-the-art methods, both with and without the additional clustering step, achieving at least a 0.4 percentage point gain in LSTQ. Furthermore, we discover that the increase of runtime primarily results from the post-processing step. Without this step, ICP-4D delivers the most efficient runtime of 840 ms compared to all other methods, with only a marginal loss in performance. These observations clearly highlight that ICP-4D offers both high efficiency and strong performance, and can further benefit from improvements in the backbone network.

Effect of Sinkhorn-based Soft Matching. The Sinkhorn-based soft matching forms instance-aware point correspondence between source and target points. Owing to this strategy, it allows accurate error measurements albeit with outliers, by not being overwhelmed by the local proximity. Figure 5 visualizes the point-wise correspondences obtained from two consecutive scans, with the current scan serving as the source and the previous scan as the target. For this analysis, we extract each point segment at the initial stage of ICP, as this stage retains its geometric structure intact. As shown in the highlighted region, the nearest neighbor matching is biased toward the closest point, ignoring the

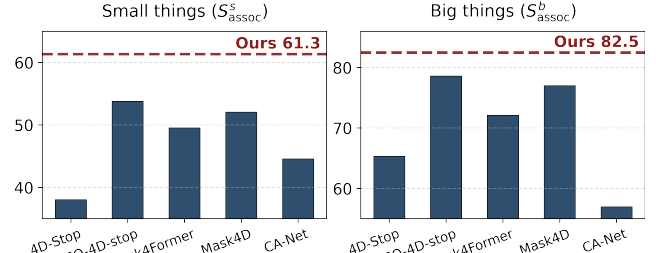


Figure 6. **Comparison of association quality by size group.**

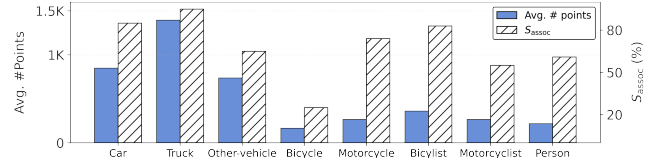


Figure 7. **Class-wise association performance.**

underlying point-wise relationships of the instance. In contrast, applying Sinkhorn-based soft matching on the baseline maintains the geometric structure, yielding correspondences that align consistently with the instance’s motion direction.

Class-wise Performance Analysis. In this section, we further analyze the effectiveness of ICP-4D w.r.t. the class over the SemanticKITTI validation set. We categorize classes with a large number of observed points (car, truck, other-vehicle) into S_{assoc}^b , whereas classes with naturally small point counts (person, bicyclist, motorcyclist, motorcycle, bicycle) are grouped into S_{assoc}^s . As shown in Figure 6, ICP-4D excels at maintaining instance consistency not only for vehicle classes but also for challenging small object classes, outperforming the baselines. Additionally, it is worth noting that all classes except bicycle exhibit favorable association performance (see Figure 7). This is attributed to the robustness of ICP-4D under scenarios where object sizes and occurrence frequencies vary significantly.

5. Conclusion

In this paper, we introduce a novel instance association strategy ICP-4D for 4D LiDAR panoptic segmentation, the first training-free framework tailored for a single scan setting. Our proposed Sinkhorn-based soft matching forming instance-aware correspondence enables ICP procedure to precisely align between two consecutive instance point segments, thereby improving temporal continuity. Additionally, we systematically design overall pipeline, underscoring the instance types to alleviate the inherent challenges of ICP and LiDAR sensors. Through experimental evaluations on both SemanticKITTI and nuScenes, our ICP-4D showcases its superiority not only on the validation sets but also on the hidden test sets, demonstrating robustness across various sensor configuration. Ultimately, our approach offers a promising direction for 4D perception by solely leveraging strong 3D panoptic models to support temporal understanding.

Limitations. Although ICP-4D shows substantial promise in advancing 4D perception, several limitations persist that warrant further investigation, particularly in real-time deployment, handling partial LiDAR observations, and dependence on camera parameters. We provide additional discussions in the supplementary materials.

References

- [1] Ali Athar, Enxu Li, Sergio Casas, and Raquel Urtasun. 4d-former: Multimodal 4d panoptic segmentation. In *Conference on Robot Learning*, pages 2151–2164. PMLR, 2023. [1](#)
- [2] Mehmet Aygun, Aljosa Osep, Mark Weber, Maxim Maximov, Cyrill Stachniss, Jens Behley, and Laura Leal-Taixe. 4d panoptic lidar segmentation. In *Proceedings of the IEEE/CVF Conference on Computer Vision and Pattern Recognition (CVPR)*, pages 5527–5537, 2021. [1, 2, 5, 3](#)
- [3] Mokhtar S Bazaraa, John J Jarvis, and Hanif D Sherali. *Linear programming and network flows*. John Wiley & Sons, 2011. [2](#)
- [4] Jens Behley, Martin Garbade, Andres Milioto, Jan Quenzel, Sven Behnke, Cyrill Stachniss, and Jurgen Gall. Semantickitti: A dataset for semantic scene understanding of lidar sequences. In *Proceedings of the IEEE/CVF international conference on computer vision*, pages 9297–9307, 2019. [2, 5, 3, 4](#)
- [5] Jon Louis Bentley. Multidimensional binary search trees used for associative searching. *Communications of the ACM*, 18(9):509–517, 1975. [3, 4](#)
- [6] Paul J Besl and Neil D McKay. Method for registration of 3-d shapes. In *Sensor fusion IV: control paradigms and data structures*, pages 586–606. Spie, 1992. [3](#)
- [7] Alex Bewley, Zongyuan Ge, Lionel Ott, Fabio Ramos, and Ben Upcroft. Simple online and realtime tracking. In *2016 IEEE international conference on image processing (ICIP)*, pages 3464–3468. Ieee, 2016. [1, 2](#)
- [8] Sofen Bouaziz, Andrea Tagliasacchi, and Mark Pauly. Sparse iterative closest point. In *Computer graphics forum*, pages 113–123. Wiley Online Library, 2013. [3](#)
- [9] Alvaro Parra Bustos and Tat-Jun Chin. Guaranteed outlier removal for point cloud registration with correspondences. *IEEE transactions on pattern analysis and machine intelligence*, 40(12):2868–2882, 2017. [3](#)
- [10] Ricardo JGB Campello, Davoud Moulavi, and Jörg Sander. Density-based clustering based on hierarchical density estimates. In *Pacific-Asia conference on knowledge discovery and data mining*, pages 160–172. Springer, 2013. [7, 8](#)
- [11] Christopher Choy, Wei Dong, and Vladlen Koltun. Deep global registration. In *Proceedings of the IEEE/CVF conference on computer vision and pattern recognition*, pages 2514–2523, 2020. [1, 3](#)
- [12] Marco Cuturi. Sinkhorn distances: Lightspeed computation of optimal transport. *Advances in neural information processing systems*, 26, 2013. [2, 4](#)
- [13] Whye Kit Fong, Rohit Mohan, Juana Valeria Hurtado, Lubing Zhou, Holger Caesar, Oscar Beijbom, and Abhinav Valada. Panoptic nuscenes: A large-scale benchmark for lidar panoptic segmentation and tracking. *IEEE Robotics and Automation Letters*, 7(2):3795–3802, 2022. [2, 5, 3, 4, 6](#)
- [14] Kaiming He, Georgia Gkioxari, Piotr Dollár, and Ross Girshick. Mask r-cnn. In *Proceedings of the IEEE international conference on computer vision*, pages 2961–2969, 2017. [2](#)
- [15] Fangzhou Hong, Hui Zhou, Xinge Zhu, Hongsheng Li, and Ziwei Liu. Lidar-based panoptic segmentation via dynamic shifting network. In *Proceedings of the IEEE/CVF conference on computer vision and pattern recognition*, pages 13090–13099, 2021. [2, 3, 5](#)
- [16] Fangzhou Hong, Lingdong Kong, Hui Zhou, Xinge Zhu, Hongsheng Li, and Ziwei Liu. Unified 3d and 4d panoptic segmentation via dynamic shifting networks. *IEEE Transactions on Pattern Analysis and Machine Intelligence*, 46(5):3480–3495, 2024. [1, 2](#)
- [17] Juana Valeria Hurtado, Rohit Mohan, Wolfram Burgard, and Abhinav Valada. Mopt: Multi-object panoptic tracking. *arXiv preprint arXiv:2004.08189*, 2020. [1, 3](#)
- [18] Rudolph Emil Kalman. A new approach to linear filtering and prediction problems. 1960. [2](#)
- [19] Alexander Kirillov, Kaiming He, Ross Girshick, Carsten Rother, and Piotr Dollár. Panoptic segmentation. In *Proceedings of the IEEE/CVF conference on computer vision and pattern recognition*, pages 9404–9413, 2019. [1](#)
- [20] Lars Kreuzberg, Idil Esen Zulfikar, Sabarinath Mahadevan, Francis Engelmann, and Bastian Leibe. 4d-stop: Panoptic segmentation of 4d lidar using spatio-temporal object proposal generation and aggregation. In *European Conference on Computer Vision*, pages 537–553. Springer, 2022. [1, 2, 5, 3, 4](#)
- [21] Harold W Kuhn. The hungarian method for the assignment problem. *Naval research logistics quarterly*, 2(1-2):83–97, 1955. [4](#)
- [22] Xin Lai, Jianhui Liu, Li Jiang, Liwei Wang, Hengshuang Zhao, Shu Liu, Xiaojuan Qi, and Jiaya Jia. Stratified transformer for 3d point cloud segmentation. In *Proceedings of the IEEE/CVF conference on computer vision and pattern recognition*, pages 8500–8509, 2022. [1](#)
- [23] Alex H Lang, Sourabh Vora, Holger Caesar, Lubing Zhou, Jiong Yang, and Oscar Beijbom. Pointpillars: Fast encoders for object detection from point clouds. In *Proceedings of the IEEE/CVF conference on computer vision and pattern recognition*, pages 12697–12705, 2019. [5](#)
- [24] Jiayuan Li. A practical $o(n^2)$ outlier removal method for correspondence-based point cloud registration. *IEEE Transactions on Pattern Analysis and Machine Intelligence*, 44(8):3926–3939, 2021. [3](#)
- [25] Jinke Li, Xiao He, Yang Wen, Yuan Gao, Xiaoqiang Cheng, and Dan Zhang. Panoptic-phnet: Towards real-time and high-precision lidar panoptic segmentation via clustering pseudo heatmap. In *Proceedings of the IEEE/CVF conference on computer vision and pattern recognition*, pages 11809–11818, 2022. [2](#)
- [26] Yancong Lin and Holger Caesar. Icp-flow: Lidar scene flow estimation with icp. In *Proceedings of the IEEE/CVF Conference on Computer Vision and Pattern Recognition*, pages 15501–15511, 2024. [3, 4, 7](#)
- [27] Huanyu Liu, Chao Peng, Changqian Yu, Jingbo Wang, Xu Liu, Gang Yu, and Wei Jiang. An end-to-end network for

panoptic segmentation. In *Proceedings of the IEEE/CVF conference on computer vision and pattern recognition*, pages 6172–6181, 2019. 2

[28] Zhijian Liu, Xinyu Yang, Haotian Tang, Shang Yang, and Song Han. Flatformer: Flattened window attention for efficient point cloud transformer. In *Proceedings of the IEEE/CVF conference on computer vision and pattern recognition*, pages 1200–1211, 2023. 1

[29] Rodrigo Marcuzzi, Lucas Nunes, Louis Wiesmann, Ignacio Vizzo, Jens Behley, and Cyrill Stachniss. Contrastive instance association for 4d panoptic segmentation using sequences of 3d lidar scans. *IEEE Robotics and Automation Letters*, 7(2):1550–1557, 2022. 1, 2, 5, 3, 4

[30] Rodrigo Marcuzzi, Lucas Nunes, Louis Wiesmann, Elias Marks, Jens Behley, and Cyrill Stachniss. Mask4d: End-to-end mask-based 4d panoptic segmentation for lidar sequences. *IEEE Robotics and Automation Letters*, 8(11):7487–7494, 2023. 1, 2, 5, 3, 4

[31] Tim Meinhardt, Alexander Kirillov, Laura Leal-Taixe, and Christoph Feichtenhofer. Trackformer: Multi-object tracking with transformers. In *Proceedings of the IEEE/CVF conference on computer vision and pattern recognition*, pages 8844–8854, 2022. 1, 2

[32] Andres Milioto, Jens Behley, Chris McCool, and Cyrill Stachniss. Lidar panoptic segmentation for autonomous driving. In *2020 IEEE/RSJ International Conference on Intelligent Robots and Systems (IROS)*, pages 8505–8512. IEEE, 2020. 1

[33] Himangi Mittal, Brian Okorn, and David Held. Just go with the flow: Self-supervised scene flow estimation. In *Proceedings of the IEEE/CVF conference on computer vision and pattern recognition*, pages 11177–11185, 2020. 5

[34] Rohit Mohan and Abhinav Valada. Efficientps: Efficient panoptic segmentation. *International Journal of Computer Vision*, 129(5):1551–1579, 2021. 2

[35] Ziqi Pang, Zhichao Li, and Naiyan Wang. Simpletrack: Understanding and rethinking 3d multi-object tracking. In *European Conference on Computer Vision*, pages 680–696. Springer, 2022. 2

[36] Zheng Qin, Le Wang, Sanping Zhou, Panpan Fu, Gang Hua, and Wei Tang. Towards generalizable multi-object tracking. In *Proceedings of the IEEE/CVF Conference on Computer Vision and Pattern Recognition*, pages 18995–19004, 2024. 1, 2

[37] Ryan Razani, Ran Cheng, Enxu Li, Ehsan Taghavi, Yuan Ren, and Liu Bingbing. Gp-s3net: Graph-based panoptic sparse semantic segmentation network. In *Proceedings of the IEEE/CVF international conference on computer vision*, pages 16076–16085, 2021. 2

[38] Szymon Rusinkiewicz and Marc Levoy. Efficient variants of the icp algorithm. In *Proceedings third international conference on 3-D digital imaging and modeling*, pages 145–152. IEEE, 2001. 3

[39] Radu Bogdan Rusu, Nico Blodow, and Michael Beetz. Fast point feature histograms (fpfh) for 3d registration. In *2009 IEEE international conference on robotics and automation*, pages 3212–3217. IEEE, 2009. 3

[40] Aleksandr Segal, Dirk Haehnel, and Sebastian Thrun. Generalized-icp. In *Robotics: science and systems*, page 435. Seattle, WA, 2009. 3

[41] Mattia Segu, Luigi Piccinelli, Siyuan Li, Yung-Hsu Yang, Bernt Schiele, and Luc Van Gool. Samba: Synchronized set-of-sequences modeling for multiple object tracking. *arXiv preprint arXiv:2410.01806*, 2024. 1

[42] Richard Sinkhorn. Diagonal equivalence to matrices with prescribed row and column sums. *The American Mathematical Monthly*, 74(4):402–405, 1967. 4

[43] Hugues Thomas, Charles R Qi, Jean-Emmanuel Deschaud, Beatriz Marcotegui, Fran ois Goulette, and Leonidas J Guibas. Kpconv: Flexible and deformable convolution for point clouds. In *Proceedings of the IEEE/CVF international conference on computer vision*, pages 6411–6420, 2019. 5

[44] C dric Villani et al. *Optimal transport: old and new*. Springer, 2008. 2

[45] Paul Voigtlaender, Michael Krause, Aljosa Osep, Jonathon Luiten, Berin Balachandar Gnana Sekar, Andreas Geiger, and Bastian Leibe. Mots: Multi-object tracking and segmentation. In *Proceedings of the ieee/cvf conference on computer vision and pattern recognition*, pages 7942–7951, 2019. 1, 3

[46] Yue Wang and Justin M Solomon. Deep closest point: Learning representations for point cloud registration. In *Proceedings of the IEEE/CVF international conference on computer vision*, pages 3523–3532, 2019. 1, 3

[47] Xinshuo Weng, Jianren Wang, David Held, and Kris Kitani. 3d multi-object tracking: A baseline and new evaluation metrics. In *2020 IEEE/RSJ International Conference on Intelligent Robots and Systems (IROS)*, pages 10359–10366. IEEE, 2020. 5

[48] Xinshuo Weng, Jianren Wang, David Held, and Kris Kitani. Ab3dmot: A baseline for 3d multi-object tracking and new evaluation metrics. *arXiv preprint arXiv:2008.08063*, 2020. 2

[49] Nicolai Wojke, Alex Bewley, and Dietrich Paulus. Simple online and realtime tracking with a deep association metric. In *2017 IEEE international conference on image processing (ICIP)*, pages 3645–3649. IEEE, 2017. 1, 2

[50] Xiaoyang Wu, Yixing Lao, Li Jiang, Xihui Liu, and Hengshuang Zhao. Point transformer v2: Grouped vector attention and partition-based pooling. *Advances in Neural Information Processing Systems*, 35:33330–33342, 2022. 1

[51] Xiaoyang Wu, Li Jiang, Peng-Shuai Wang, Zhijian Liu, Xihui Liu, Yu Qiao, Wanli Ouyang, Tong He, and Hengshuang Zhao. Point transformer v3: Simpler faster stronger. In *Proceedings of the IEEE/CVF conference on computer vision and pattern recognition*, pages 4840–4851, 2024. 1

[52] Yuwen Xiong, Renjie Liao, Hengshuang Zhao, Rui Hu, Min Bai, Ersin Yumer, and Raquel Urtasun. Upsnet: A unified panoptic segmentation network. In *Proceedings of the IEEE/CVF conference on computer vision and pattern recognition*, pages 8818–8826, 2019. 2

[53] Jiaolong Yang, Hongdong Li, Dylan Campbell, and Yunde Jia. Go-icp: A globally optimal solution to 3d icp point-set registration. *IEEE transactions on pattern analysis and machine intelligence*, 38(11):2241–2254, 2015. 3

[54] Kadir Yilmaz, Jonas Schult, Alexey Nekrasov, and Bastian Leibe. Mask4former: Mask transformer for 4d panoptic segmentation. In *2024 IEEE International Conference on Robotics and Automation (ICRA)*, pages 9418–9425. IEEE, 2024. [1](#), [2](#), [3](#), [5](#), [4](#)

[55] Fangao Zeng, Bin Dong, Yuang Zhang, Tiancai Wang, Xiangyu Zhang, and Yichen Wei. Motr: End-to-end multiple-object tracking with transformer. In *European conference on computer vision*, pages 659–675. Springer, 2022. [1](#), [2](#)

[56] Tianyuan Zhang, Xuanyao Chen, Yue Wang, Yilun Wang, and Hang Zhao. Mutr3d: A multi-camera tracking framework via 3d-to-2d queries. In *Proceedings of the IEEE/CVF Conference on Computer Vision and Pattern Recognition*, pages 4537–4546, 2022. [2](#)

[57] Xiyu Zhang, Jiaqi Yang, Shikun Zhang, and Yanning Zhang. 3d registration with maximal cliques. In *Proceedings of the IEEE/CVF conference on computer vision and pattern recognition*, pages 17745–17754, 2023. [1](#), [3](#)

[58] Yifu Zhang, Peize Sun, Yi Jiang, Dongdong Yu, Fucheng Weng, Zehuan Yuan, Ping Luo, Wenyu Liu, and Xinggang Wang. Bytetrack: Multi-object tracking by associating every detection box. In *European conference on computer vision*, pages 1–21. Springer, 2022. [1](#), [2](#)

[59] Yuang Zhang, Tiancai Wang, and Xiangyu Zhang. Motrv2: Bootstrapping end-to-end multi-object tracking by pretrained object detectors. In *Proceedings of the IEEE/CVF conference on computer vision and pattern recognition*, pages 22056–22065, 2023. [1](#), [2](#)

[60] Yushan Zhang, Aljoša Ošep, Laura Leal-Taixé, and Tim Meinhardt. Zero-shot 4d lidar panoptic segmentation. In *Proceedings of the Computer Vision and Pattern Recognition Conference*, pages 24506–24517, 2025. [2](#)

[61] Xingyi Zhou, Vladlen Koltun, and Philipp Krähenbühl. Tracking objects as points. In *European conference on computer vision*, pages 474–490. Springer, 2020. [2](#)

[62] Zixiang Zhou, Yang Zhang, and Hassan Foroosh. Panoptic-polarnet: Proposal-free lidar point cloud panoptic segmentation. In *Proceedings of the IEEE/CVF conference on computer vision and pattern recognition*, pages 13194–13203, 2021. [2](#)

[63] Minghan Zhu, Shizhong Han, Hong Cai, Shubhankar Borse, Maani Ghaffari, and Fatih Porikli. 4d panoptic segmentation as invariant and equivariant field prediction. In *Proceedings of the IEEE/CVF International Conference on Computer Vision*, pages 22488–22498, 2023. [1](#), [2](#), [5](#), [3](#), [4](#)

[64] Xizhou Zhu, Weijie Su, Lewei Lu, Bin Li, Xiaogang Wang, and Jifeng Dai. Deformable detr: Deformable transformers for end-to-end object detection. *arXiv preprint arXiv:2010.04159*, 2020. [2](#)

ICP-4D: Bridging Iterative Closest Point and LiDAR Panoptic Segmentation

Supplementary Material

A. Implementation Details

A.1. Baseline Details

In this section, we provide a detailed overview of the strong baselines considered in our comparison: 4D-PLS [2] (CVPR’21), 4D-Stop (ECCVW’22) [20], EQ-4D-Stop (ICCV’23) [63], CA-Net (R-AL’22) [29], Mask4D (R-AL’23) [30], and Mask4Former (ICRA’24) [54]. Note that we report the official results as stated in the original papers, and reproduce the results when formal reports are not available. The following paragraph details the experimental settings and notable modifications for each baseline.

First, 4D-PLS, 4D-Stop, and EQ-4D-Stop follow a two-stage design, where instance tracklets are first generated independently for all scans and then stitched across consecutive frames. Accordingly, we measure the inference time of each stage separately and report their average as the overall runtime. Second, Mask4Former is originally developed for 4D LiDAR panoptic segmentation with superimposed point clouds. To establish a strong baseline for our experiments, we train it as a 3D panoptic network without any modifications, except setting the number of input scans to one. Third, CA-Net employs contrastive learning for instance association on top of an off-the-shelf 3D panoptic segmentation network. For a fair comparison, we integrate the single scan Mask4Former into the CA-Net framework. Since CA-Net requires point-wise instance features for contrastive learning, we extract them by computing the dot product between instance queries and instance masks. Lastly, official panoptic nuScenes results are unavailable for any methods except 4D-Stop and EQ-4D-Stop. Therefore, we additionally reproduce the remaining baselines using their official repositories, following the experimental protocol of EQ-4D-StOP.

A.2. Metrics

In this section, we provide detailed explanations of the metrics employed for evaluating association performance in our experiments. While LSTQ is the most widely used metric, we additionally report two complementary metrics, MOTSA and PTQ, to provide a more comprehensive assessment.

LSTQ [2] is delicately designed to evaluate 4D panoptic segmentation quality. First, to assess the semantic segmentation performance over the classes C , the classification score S_{cls} is defined as:

$$S_{cls} = \frac{1}{|C|} \sum_{c=1}^C \frac{|\text{TP}_c|}{|\text{TP}_c| + |\text{FN}_c| + |\text{FP}_c|} = \frac{1}{C} \sum_{c=1}^C \text{IoU}(c), \quad (10)$$

where TP, FN, and FP denote the true positives, false negatives, and false positives, respectively. Furthermore, the association score S_{assoc} , which is responsible for measuring temporal continuity, is defined as:

$$S_{assoc} = \frac{1}{|I|} \sum_{t \in I} \frac{1}{|gt_{id}(t)|} \sum_{s \in S, s \cap t \neq \emptyset} TPA(s, t) \text{IoU}(s, t), \quad (11)$$

where I and S refer to the ground-truth and predicted segments. Note that TPA represents the points that maintain consistent identities across scans, regardless of class. Consequently, LSTQ is computed as the geometric mean of the classification score S_{cls} and association score S_{assoc} .

MOTSA & sMOTSA [45] are mask-based variants of the widely used Multi-Object Tracking Accuracy (MOTA) metric, replacing bounding-box overlaps with mask IoU to better evaluate segmentation-level tracking performance. Formally,

$$\text{MOTSA} = \frac{|\text{TP}| - |\text{FP}| - |\text{IDSW}|}{|M|}, \quad (12)$$

where $|\text{IDSW}|$ denotes the total number of ID switches, and $|M|$ is the number of ground truth segmentation masks. In addition, sMOTSA replaces the true positive (TP) with soft true positive (sTP), obtained by accumulating the mask IoUs over all matched predictions.

PTQ & sPTQ [17] are formulated to satisfy the fundamental requirement that panoptic tracking metrics must jointly capture segmentation accuracy and tracking consistency over time. Thus, they incorporate an ID-switch penalty into the original Panoptic Quality (PQ) measure, as follows:

$$\text{PTQ} = \frac{1}{|C|} \sum_{c=1}^C \frac{\sum_{(s,t) \in \text{TP}_c} \text{IoU}(s, t) - |\text{IDSW}_c|}{|\text{TP}_c| + \frac{1}{2}|\text{FP}_c| + \frac{1}{2}|\text{FN}_c|}. \quad (13)$$

Furthermore, sPTQ leverages the soft version of IDSW (sIDSW) instead of IDSW. This soft variant aggregates the IoU scores for segments in which the predicted instance ID ID changes:

$$s\text{IDSW}_c = \{\text{IoU}(s, t) \mid (s, t) \in \text{TP}_c \wedge ID_s \neq ID_t\}. \quad (14)$$

B. Method Details

B.1. Pipeline Details

The overall association pipeline of our proposed ICP-4D is summarized in Algorithm 1. We apply ICP-4D sequentially across all scans within each sequence, and reset the memory bank \mathcal{B} at the beginning of every new sequence.

Algorithm 1 Instance association process of ICP-4D

Require: Instance predictions \mathcal{I} , semantic predictions \mathcal{S} , memory bank \mathcal{B}

- 1: **for** time step $t \in \{1, 2, \dots, T-1\}$ **do**
- 2: Construct the candidate set $\mathcal{M} = \mathcal{G}'_{\text{src}} \times \mathcal{G}'_{\text{dst}}$ filtered by semantic predictions \mathcal{S} .
- // **Static instances (Sec. 3.2.1)**
- 3: Associate instances using the center μ of each point set (Eq. 4).
- 4: Refine the matched pairs using the covariance descriptor σ (Eq. 6).
- // **Dynamic instances (Sec. 3.2.2)**
- 5: Perform dynamic instance association using ICP enhanced with *Sinkhorn-based soft matching*.
- // **Missing instances (Sec. 3.2.3)**
- 6: **if** \mathcal{B} is not empty **then**
- 7: Apply the dynamic matching procedure (Lines 5) to missing instances.
- 8: **end if**
- 9: Update the memory bank \mathcal{B} .
- 10: **end for**

Ensure: Consistent instance IDs across the entire sequence.

B.2. Complexity Analysis

In this section, we provide a computational complexity comparison between Sinkhorn-based soft matching and nearest neighbor-based matching. As described in Section 3.2.2, we utilize the entropy-regularized optimal transport problem [12] to obtain instance-aware point correspondences. Before analyzing the regularized form, we briefly review the optimal transport problem. Given two probability vectors $r \in \mathbb{R}_+^n$ and $c \in \mathbb{R}_+^m$, the original optimal transport problem [44] aims to find the optimal transport plan $\mathcal{Q} \in U(r, c)$. The entries of \mathcal{Q} represent the amount of mass transported from the i -th element of r to the j -th element of c . The transport polytope U is defined as:

$$U(r, c) = \{Q \in \mathbb{R}_+^{n \times m} \mid \sum_j Q_{ij} = r_i, \forall i, \sum_i Q_{ij} = c_j, \forall j\}. \quad (15)$$

Let \mathcal{Z} denote the transport cost matrix. The optimal transport plan is then computed as the Frobenius inner product between \mathcal{Q} and \mathcal{Z} :

$$\text{OT}(r, c) := \min_{\mathcal{Q}} \langle \mathcal{Z}, \mathcal{Q} \rangle_F. \quad (16)$$

This optimization is a linear program, for which the network simplex [3] is the most widely used exact solver. In the symmetric case $n = m$, its worst-case computational complexity scales as $O(n^3 \log n)$. However, due to its heavy computational cost, adding an entropic regularization is widely

Table A.1. **Comparison Between Nearest Neighbor and Sinkhorn-based Matching.** We report the results of our full ICP-4D when integrating each correspondence strategy.

w/ Nearest Neighbor (KD-Tree)		w/ Sink.-based Soft Matching	
LSTQ	Inf. Time (s)	LSTQ	Inf. Time (s)
72.1	2.01	72.7	2.35

Table A.2. **SemanticKITTI [4] Test Set Leaderboard (Top 5).** mAQ and mIoU denote the S_{assoc} and S_{cls} , respectively.

Rank	User	LSTQ \uparrow	mAQ \uparrow	mIoU \uparrow
1	ICP-4D (Ours)	70.3	70.0	70.5
2	YAKD	68.6	70.8	66.5
3	hphnngcquan	68.5	70.4	66.7
4	KadirYilmaz	68.4	67.3	69.6
5	ConOcc	67.9	68.3	67.4

adopted to accelerate optimal transport. By incorporating the Shannon entropy $H(\mathcal{Q}) := -\sum_{i,j} \mathcal{Q}_{ij} \log \mathcal{Q}_{ij}$ into Eq. 16, we obtain the entropy-regularized optimal transport formulation. To handle marginal constraints, we introduce dual variables $f \in \mathbb{R}^n$ and $g \in \mathbb{R}^m$ and form the corresponding Lagrangian. Then, by taking the first-order optimality condition, we find that optimal solution \mathcal{Q} has matrix form $\mathcal{Q} = \text{diag}(u)K\text{diag}(v)$, where $u_i = e^{f_i/\epsilon}$, $v_j = e^{g_j/\epsilon}$, and $K_{ij} = e^{-Z_{ij}/\epsilon}$. Since u and v must satisfy the marginal constraints, the entropic regularization transforms the classical optimal transport problem from a linear program into a matrix scaling problem. Thus, when $n = m$, the computational complexity is reduced to $O(n^2)$. However, the nearest neighbor algorithm operates in $O(n \log n)$ on average and up to $O(n^2)$ in the worst case in practice, as implemented in the scikit-learn library (e.g., using KD-Tree [5]). Consequently, our Sinkhorn-based solution is theoretically comparable to the nearest neighbor algorithm, and the wall-clock time shows only a marginal difference while achieving higher performance (see Table A.1).

C. Additional Experimental Results

C.1. Leaderboard Results

Table A.2 shows the SemanticKITTI [4] challenge leaderboard ranks on the hidden test set, ordered by LSTQ. In this leaderboard, we observe that our proposed ICP-4D outperforms not only all published methods but also every competition participant. Specifically, we achieve 1st place in LSTQ as of submission date. These results demonstrate the strong generalization capability and practical effectiveness of our method under challenging scenarios.

Table A.3. Analysis on performance over the number of superimposed scans.

Method	# Scan	Memory (GB)	Time (s)	Validation set					Test set				
				LSTQ	S _{assoc}	S _{cls}	IoU St	IoU Th	LSTQ	S _{assoc}	S _{cls}	IoU St	IoU Th
(a) IoU-based Association													
4D-PLS [2]	2	-	-	59.9	58.8	61.0	65.0	63.1	-	-	-	-	-
	4	8.0	3.48	62.7	65.1	60.5	65.4	61.3	56.9	56.4	57.4	66.9	51.6
4D-Stop [20]	2	15.9	3.67	66.4	71.8	61.4	64.9	64.1	62.9	67.3	58.8	68.3	53.3
	4	18.9	4.32	67.0	74.4	60.3	65.3	60.9	63.9	69.5	58.8	67.7	53.8
Eq-4D-Stop [63]	2	11.3	2.89	68.9	74.8	63.5	65.7	68.4	65.4	69.7	61.5	68.7	59.1
	4	12.1	3.18	70.1	77.6	63.4	66.4	67.1	67.0	72.0	62.4	69.1	60.9
Mask4Former [54]	2	10.4	3.51	70.5	74.3	66.9	67.1	66.6	68.4	67.3	69.6	72.7	65.3
	4	17.1	8.56	71.9	76.3	67.8	66.9	69.0	68.0	69.7	66.3	70.7	60.3
(c) Detect & Track Association													
ICP-4D (Ours)	1	3.2	2.35	72.7	78.3	67.5	65.2	70.6	70.3	<u>70.0</u>	70.5	72.7	67.4

Table A.4. Additional comparisons across multiple metrics. () denotes the number of input scans (i.e., 1f = single, 2f = two).

Method \ Metric	MOTSA	sMOTSA	PTQ	sPTQ
4D-STOP (2f) [20]	31.0	27.1	53.4	53.7
EQ-4D-STOP (2f) [63]	43.6	39.6	56.4	56.7
Mask4D (1f) [30]	52.1	48.1	58.4	58.5
Mask4Former (2f) [54]	47.3	42.1	48.3	48.5
Mask4Former (1f)	-	-	-	-
+ CA-Net [29]	48.4	43.1	48.9	49.1
+ ICP-4D (Ours)	73.3	65.7	59.6	59.7

C.2. Additional Results

Effect of the Number of Scans. In Table A.3, we examine how well our proposed ICP-4D performs instance association with only a single scan. The number of superimposed scans is a pivotal factor influencing the association performance of the IoU-based method. Since formal reports for specific configurations are unavailable, we reproduce the results using official implementation—namely, Eq-4D-Stop [63] with 2 scans and Mask4Former [54] with 4 scans. As clearly observed in Table A.3, leveraging four superimposed scans yields a substantial improvement in S_{assoc}, with a notable sacrifice in computational efficiency. In contrast, we observe that ICP-4D exhibits superior performance, despite the absence of explicit 4D spatio-temporal volume constructed from stacked point clouds. This observation demonstrates that ICP-4D effectively associates instances using only a single scan and a 3D panoptic network, while remaining highly efficient.

Results on Multiple Metrics. We further present additional

results with multiple metrics to enable a more comprehensive comparison. MOTSA [45] is widely used for evaluating multi-object tracking and segmentation. Although MOTSA emphasizes the recognition quality rather than temporal consistency, it nonetheless offers a straightforward indicator of the ID switches. Moreover, PTQ [17] is designed to jointly evaluate panoptic segmentation and tracking quality in a holistic manner. In Table A.4, evaluations are carried out on the SemanticKITTI [4] validation set. We observe that ICP-4D consistently surpasses all baselines across multiple metrics, including LSTQ. This indicates that the strength of ICP-4D goes beyond any particular metric, offering a robust and practically reliable solution for instance association.

C.3. Hyperparameter Analysis

In this section, we examine the impact of different matching thresholds on instance association performance. Figure A.1 illustrates the LSTQ scores of ICP-4D on the SemanticKITTI [4] validation set. We empirically determine the matching thresholds { τ_{iou} , τ_{dist} , τ_{center} , τ_{cov} } over {0.1, 0.2, 0.3, 0.4, 0.5}. Here, we observe three insights. First, extremely low value of threshold τ_{iou} often yields decent performance due to over-association, whereas high thresholds lead to over-filtering and degraded matching quality. Second, excessively large τ_{center} and τ_{cov} cause static instances to be matched too liberally, leading to unreliable association. Lastly, our proposed ICP-4D delivers performance gains over all baselines, regardless of the hyperparameter choices.

C.4. Quantitative Results

We additionally provide the results of each semantic class on panoptic nuScenes [13] to facilitate a more comprehensive understanding. We present our reproduced results obtained

Table A.5. Comparison of the quantitative results on panoptic nuScenes [13].

Model	LSTQ	S_{assoc}	S_{cls}	Thing classes (AQ / IoU)										Stuff classes (IoU only)					
				barrier	bicycle	bus	car	const. veh.	motorcycle	pedestrian	traffic cone	trailer	truck	drive. surf.	other flat	sidewalk	terrain	manmade	vegetation
Mask4Former [54]	67.6	63.0	72.5	48.3/76.9	42.6/37.0	60.5/90.2	76.7/92.7	42.7/44.9	61.1/77.0	53.5/74.0	48.9/55.7	38.7/47.8	62.2/77.8	95.6	69.2	71.5	74.6	88.5	87.0
Mask4D [30]	58.5	54.1	63.1	29.7/64.3	27.8/20.5	60.5/79.2	72.5/83.5	29.5/21.8	52.5/72.0	42.3/65.9	39.5/43.0	19.2/35.2	58.9/71.8	94.2	53.9	64.9	71.3	85.2	84.5
CA-Net [29]	63.4	56.6	71.0	30.1/74.5	31.9/29.1	56.5/88.5	73.3/91.2	38.6/43.2	63.2/78.7	53.6/71.2	34.6/54.6	39.5/48.3	62.1/77.3	95.6	68.4	70.3	72.7	86.7	85.2
ICP-4D (Ours)	67.9	65.0	71.0	40.7/74.5	44.1/29.1	58.9/88.5	80.9/91.2	40.1/43.2	65.9/78.7	67.2/71.2	52.0/54.6	40.6/48.3	45.7/77.3	95.6	68.4	70.3	72.7	86.7	85.2

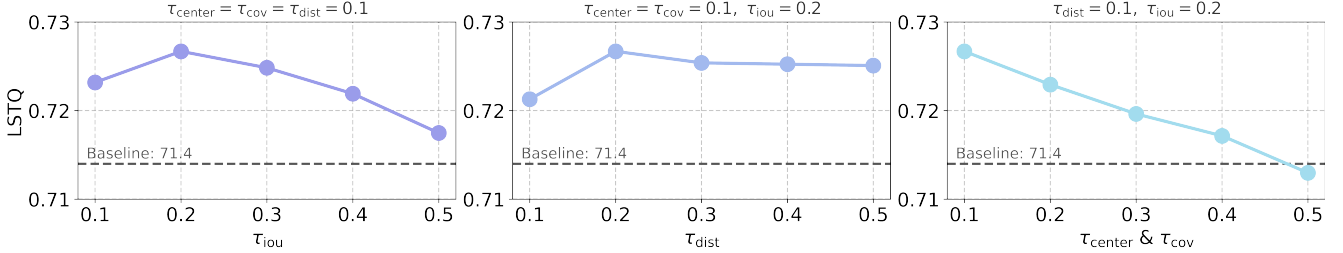


Figure A.1. Hyperparameter Analysis.

from officially given training configurations. Note that 4D-Stop [20] and EQ-4D-Stop [63] do not provide official class-wise results for the panoptic nuScenes benchmark, whereas only overall metrics such as LSTQ are available. For this reason, class-wise comparisons against these methods are excluded to avoid confusion and ensure fairness. In Table A.5, our method yields overall performance improvements, particularly in safety-critical *thing* classes (e.g., bicycle, car, and pedestrian). Furthermore, classes with relatively fewer points, such as pedestrians and traffic cones, exhibit stronger association performance against the baselines. This observation aligns with our earlier analysis on SemanticKITTI [4] presented in the main manuscript.

C.5. Qualitative Results

In this section, we present additional qualitative analysis by illustrating the results of SemanticKITTI [4] and panoptic nuScenes [13] dataset. As clearly shown in Figure A.2 and A.3, ICP-4D maintains robust ID consistency even in challenging scenarios. Our method explicitly incorporates the inherent geometric relations between instances and adopts a delicately designed pipeline that is resilient to occlusion and noisy predictions. In contrast, Mask4Former [54] associates instances by selecting the majority ID among spatially overlapped points, making it vulnerable to imprecise predictions and leading to frequent ID switches (see the 1st, 2nd, and 3rd rows of Figure A.2). Apart from this, Mask4D [30] struggles with separating nearby objects and accumulates errors from early mispredictions (see the 1st, 2nd, and 4th rows of Figure A.2). Furthermore, ICP-4D also operates well on the panoptic nuScenes dataset, which is sparse and large tempo-

ral gaps between consecutive scans. Specifically, in the 2nd and 4th rows of Figure A.3, we observe that the instances have no overlap and sparse representations. The baselines confuse the instance IDs due to their partial observations and rapid motions. However, ICP-4D successfully finds the corresponding instances even when they are distant. Also, from the 1st row of Figure A.3, we observe that ICP-4D can effectively associate instances in complex scene where pedestrians are heavily entangled.

D. Discussion

D.1. Limitation and Future work

We identify several limitations of our proposed approach, which inherits issues from both pre-trained 3D panoptic models and LiDAR sensors. While ICP-4D demonstrates strong association performance with a cost efficient pipeline, real-time deployment remains challenging. Our method highly depends on the performance of the underlying 3D panoptic model; thus, its runtime can be further improved as point cloud processing continues to advance. In addition, partial observation of instances in LiDAR sensing make it difficult to reliably associate instances. Incorporating trajectory cues represents a promising direction to further stabilize instance association. Lastly, our pipeline forces the requirement of camera parameters as a prerequisite for transforming the point coordinates into the world coordinates. Relaxing this requirement would improve the applicability of our method in broader real-world settings. We hope these insights encourage continued progress toward scalable 4D perception systems.

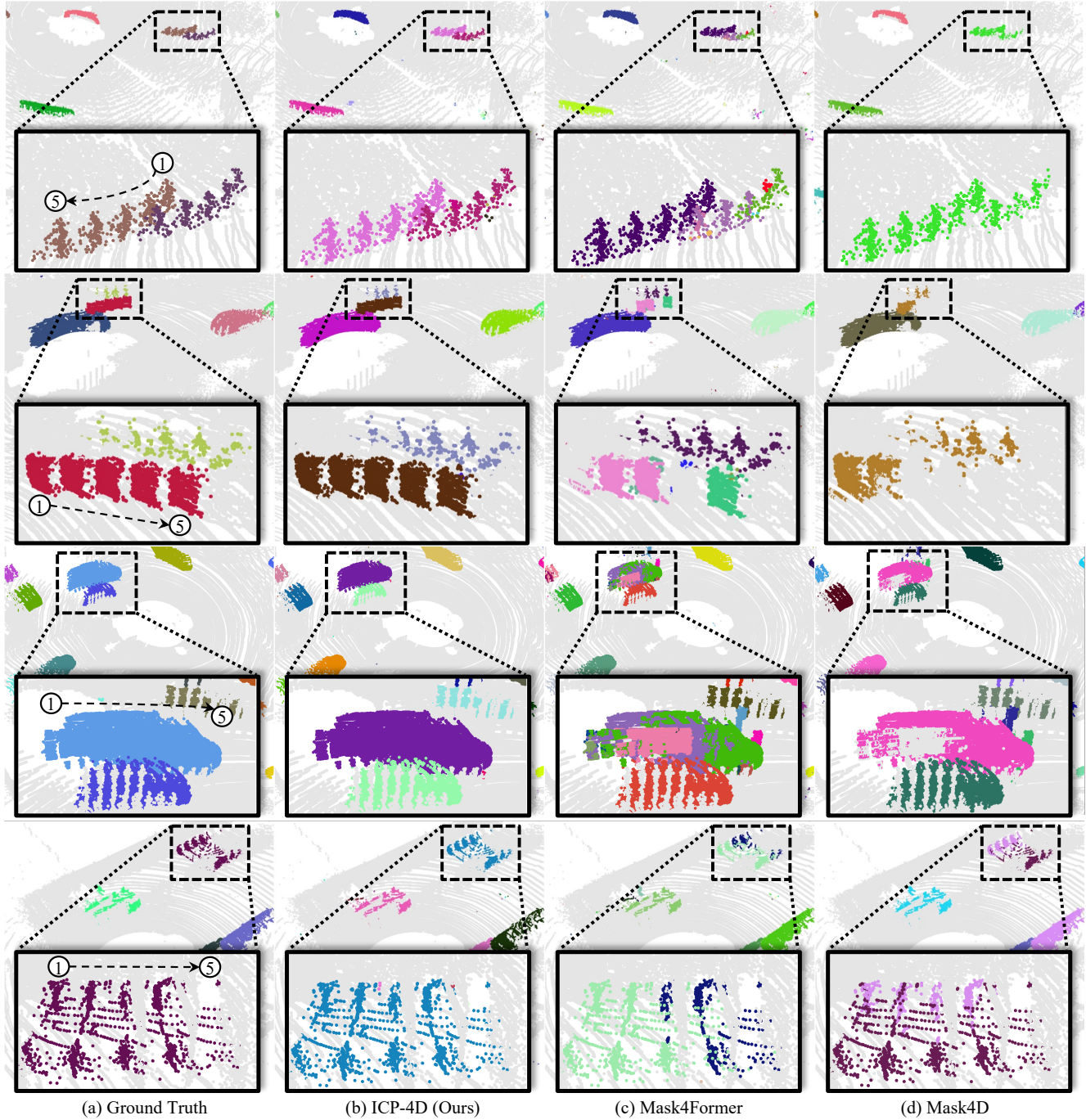


Figure A.2. **Qualitative comparison on semanticKITTI [4] validation set.** We visualize the association results over five consecutive scans for both the baselines and our ICP-4D. Different colors represent different instances. The dotted boxes zoom in for clear comparison. For clarity, we use circled numbers (①–⑤) to represent the frame indices.

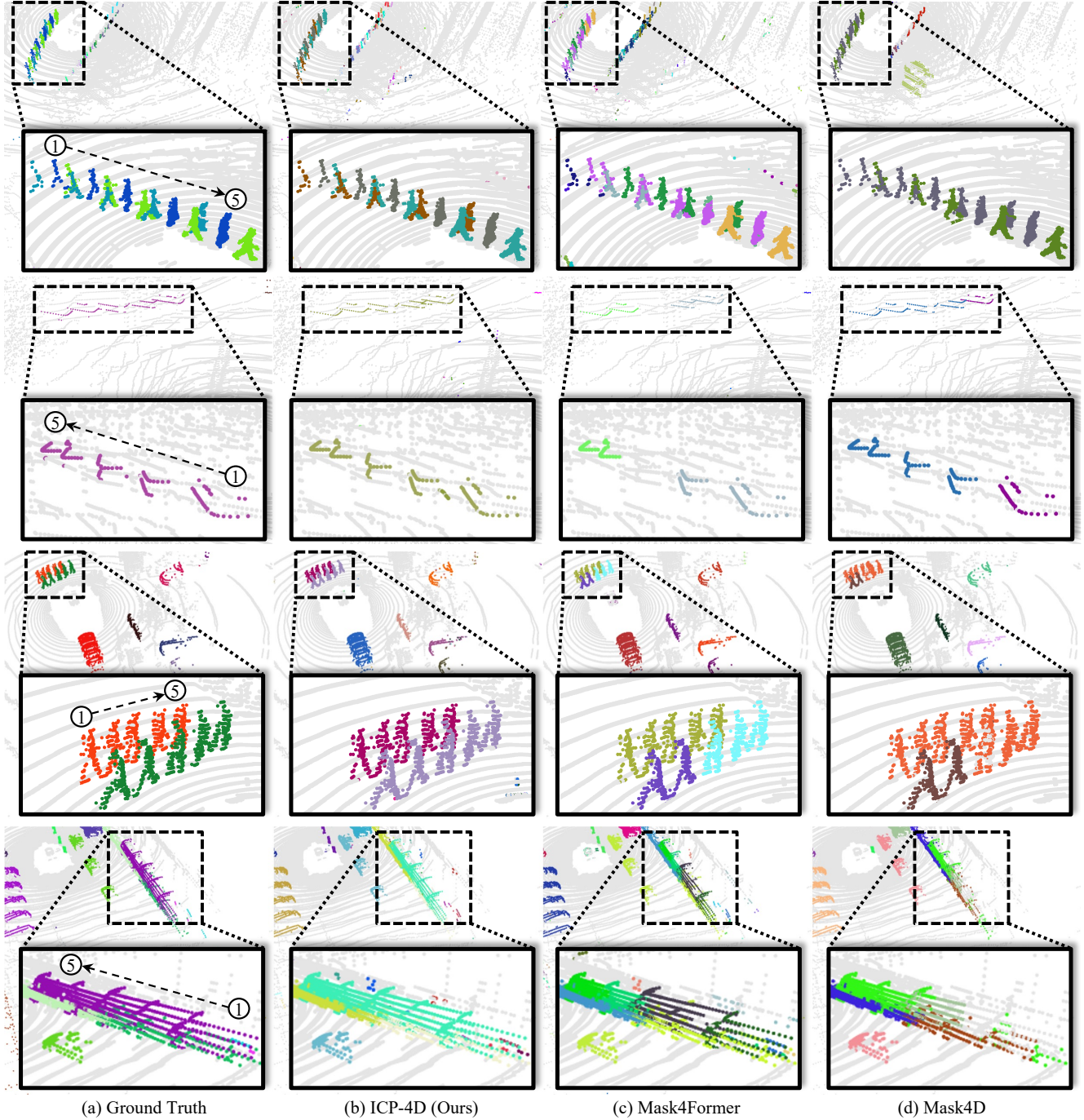


Figure A.3. **Qualitative comparison on panoptic nuScenes [13].** We visualize the association results over five consecutive scans for both the baselines and our ICP-4D. Different colors represent different instances. The dotted boxes zoom in for clear comparison. For clarity, we use circled numbers (①–⑤) to represent the frame indices.